Modeling of gain recovery of quantum cascade lasers

Muhammad Anisuzzaman Talukder[a)]
Department of Computer Science and Electrical Engineering, University of Maryland, Baltimore County, 1000 Hilltop Circle, Baltimore, Maryland 21250, USA

(Received 30 September 2010; accepted 6 December 2010; published online 4 February 2011)

We present a model to calculate the gain recovery of quantum cascade lasers (QCLs). We implement the model for two QCLs with different material systems and quantum mechanical designs. It is found that both incoherent scattering and coherent tunneling are important for gain recovery, however, their relative importance depends on the material systems, quantum mechanical designs, and operating conditions. Though details of the gain recovery vary for the two QCLs, a complete gain recovery takes ~2 ps in both cases. The results are consistent with the results found in pump-probe experiments. © *2011 American Institute of Physics*. [doi:10.1063/1.3544201]

I. INTRODUCTION

The gain of a laser directly depends on the population inversion of the lasing levels. When light that is resonant to the lasing levels propagates inside a laser cavity, the population inversion changes since the carriers radiatively scatter from one resonant level to the other. However, the population inversion recovers the equilibrium value after light leaves the medium, which is often referred to as the gain recovery since the medium recovers the ability to produce gain. The time that is required for the gain to recover is an important parameter for many applications of lasers such as creating short pulses by modelocking[1] and modulating the laser light at high-speed for optical communication.[2]

Quantum cascade lasers (QCLs) (Ref. 3) are the most promising light sources in the mid-infrared (mid-IR) range due to their small size, high output power, and agility to design at a desired wavelength in the mid-IR. QCLs have many important applications including trace gas sensing, environmental monitoring, medical diagnosis, remote sensing, and open path optical communication. Many of the promising applications require pulses that are short with high peak power and laser output modulated at a high speed. It is usually assumed that the gain recovery of QCLs is very fast, on the order of a picosecond, since the carrier transport is dominated by ultrafast electron-longitudinal optical (LO) phonon interactions.[4] The fast gain recovery of conventional QCLs makes it difficult to achieve mode-locking using conventional techniques.[5,6] On the contrary, the fast gain recovery allows QCLs to follow changes in the injection current nearly immediately without relaxation oscillations what is highly suitable for high-speed free space optical communications.[2]

QCLs are electrically pumped devices where the population inversion is obtained by electron injection into the upper lasing level and electron extraction from the lower lasing level. Therefore, the population inversion depends on the internal carrier transport through the quantized energy levels. The carrier transport in QCLs is complicated since a number of scattering processes and coherent tunneling at resonance and out of resonance are involved.[7–10] Therefore, the dynamics of the gain recovery is difficult to predict. The different transport rates also vary when quantum mechanical designs and operating conditions vary, which makes the prediction of the gain recovery even more difficult.

Till date, the gain recovery of QCLs has not been sufficiently studied. There have been limited reports of pump-probe experiments[10,11] without a detailed theoretical analysis. A theoretical analysis is important to predict the gain recovery of a designed QCL and hence determine the behavior in mode-locking or ultrafast modulation. The study of the gain recovery is also important in understanding the physics of complex multiquantum-well QCLs.

In this work, we will present a model to calculate the gain recovery of QCLs and we will implement this model to two different QCLs to understand the effects of materials and quantum mechanical designs on the gain recovery dynamics. We will show that both coherent and incoherent mechanisms play role in the gain recovery, however, their significance varies when materials and quantum mechanical designs change. The calculated gain recovery is ~2 ps at 200 K with a relatively fast recovery rate in the beginning followed by a relatively slow recovery rate in the tail. The results are consistent with the experimental observations.[10,11]

The remainder of the paper is organized as follows: in Sec. II, we will discuss the theoretical model to calculate the gain recovery of QCLs. In particular, we will present a model to calculate the carrier transport in QCLs including both the incoherent scattering and coherent tunneling mechanisms; we will present a model to calculate the interactions of the carrier densities with the pump pulse; and we will present models to calculate the scattering and coherence lifetimes. In Sec. III, we will present the results that we obtained from the implementation of the gain recovery model to two QCLs. Finally, in Sec. IV, we will summarize the results and draw conclusions.

II. THEORETICAL MODEL

In practice, the gain recovery of a laser is estimated using the so called pump-probe experiments.[12] In a pump-probe experiment, a strong pump pulse, which is resonant to

a)Electronic mail: anisuzzaman@umbc.edu.

the lasing levels, is injection-locked into the laser. If the lasing levels are inverted at equilibrium, the pump pulse depletes the upper lasing level by radiative scattering of the carriers to the lower lasing level. By contrast, if the lasing levels are uninverted at equilibrium, the pump pulse depletes the lower lasing level by radiative scattering of the carriers to the upper lasing level. When the pump pulse leaves the medium, the carrier densities of both the lasing levels relax and recover the equilibrium values. A weak probe pulse is propagated through the laser with varying delays to the pump pulse. The probe pulse experiences a variable gain when its position with respect to the pump pulse changes since the inversion changes due to interaction with the pump pulse and the recovery takes finite time. If the probe pulse leads the pump pulse in time in an initially inverted medium, it experiences a constant gain. In presence of the pump pulse, the probe pulse experiences a sharp decrease in gain. When the probe pulse lags the pump pulse, it experiences a rise or recovery of gain. The differential gain measured from the received probe pulse is used to estimate the gain recovery.

In our model, we use a similar approach. First, we calculate the equilibrium carrier densities in the energy levels for a given design and operating conditions. Then, we excite the lasing levels by a narrow, strong, and resonant pump pulse. We calculate the interactions of the carrier densities with the pump pulse and the recovery of the carrier densities after the pump pulse leaves the medium. We do not need a probe pulse since we directly calculate the recovery of the carrier densities.

A. Density equations

A number of different approaches have been used to calculate carrier transport in QCLs.[13–16] In this work, we use an extended density matrix formalism, similar to the one that has been discussed in Ref. 17, which includes carrier transport due to both incoherent scattering and coherent tunneling. We write the density equations as

$$\frac{dn_x}{dt} = \sum_{x' \neq x} \frac{n_{x'}}{s_{x'x}} - \sum_{x' \neq x} \frac{n_x}{s_{xx'}} - i \sum_{x' \neq x} \frac{\Delta_{0,xx'}}{2\hbar}(C_{xx'} - C^*_{xx'}), \tag{1a}$$

$$\frac{dC_{xx'}}{dt} = i\frac{\Delta_{0,xx'}}{2\hbar}(n_{x'} - n_x) - \frac{C_{xx'}}{T_{2,xx'}} - i\frac{E_{xx'}}{\hbar}C_{xx'}. \tag{1b}$$

In Eq. (1), the quantity n is the carrier density. Subscript x denotes an energy level. The quantity $C_{xx'}$ denotes the coherence between the energy levels x and x'. The coherence $C_{xx'}$ has a nonzero value only between an injector level and an active region level. The quantities $s_{xx'}$ and $T_{2,xx'}$ denote the scattering and coherence times between the energy levels x and x'. The parameter $\Delta_{0,xx'}$ denotes the energy splitting at resonance between the energy levels x and x' involved in coherent tunneling. Therefore, the parameter $\Delta_{0,xx'}$ is the minimum energy spacing between the injector and active region levels at injection and extraction barriers. The parameter $E_{xx'}$ denotes the detuning of the energies of the levels x and x' from resonance so that $E_{xx'} = \|E_x - E_{x'}| - \Delta_{0,xx'}|$, where E_x and $E_{x'}$ are the energies of the levels x and x', respectively. In our model, we formulate and solve the density equations for one active region and two injector regions preceding and following the active region assuming translational symmetry and hence taking periodic boundary conditions.

B. Interactions with the pump pulse

The interactions of the carrier densities of the lasing levels with the pump pulse are calculated by adding the Bloch equations to Eq. (1).[18] Therefore, the density equations for the upper lasing (ul) level and the lower lasing (ll) level change to

$$\frac{dn_{x=\mathrm{ul}}}{dt} = \sum_{x' \neq x} \frac{n_{x'}}{s_{x'x}} - \sum_{x' \neq x} \frac{n_x}{s_{xx'}} - i \sum_{x' \neq x} \frac{\Delta_{0,xx'}}{2\hbar}(C_{xx'} - C^*_{xx'}) + i\frac{\mu}{2\hbar}(\eta\mathcal{E}^* - \eta^*\mathcal{E}), \tag{2a}$$

$$\frac{dn_{x=\mathrm{ll}}}{dt} = \sum_{x' \neq x} \frac{n_{x'}}{s_{x'x}} - \sum_{x' \neq x} \frac{n_x}{s_{xx'}} - i \sum_{x' \neq x} \frac{\Delta_{0,xx'}}{2\hbar}(C_{xx'} - C^*_{xx'}) - i\frac{\mu}{2\hbar}(\eta\mathcal{E}^* - \eta^*\mathcal{E}). \tag{2b}$$

In Eq. (2), the parameter μ is the dipole moment between the resonant levels. The parameters $\mathcal{E}$ and η are the envelope of electric field and polarization. The evolution of η is given by[18]

$$\frac{\partial \eta}{\partial t} = i\frac{\mu}{2\hbar}(n_{x=\mathrm{ul}} - n_{x=\mathrm{ll}})\mathcal{E} - \frac{\eta}{T_{2,\mathrm{ul\text{-}ll}}}. \tag{3}$$

For the pump pulse, we choose $\mathcal{E} = \mathcal{E}_m \,\mathrm{sech}(t/\tau)$, where τ is the full width half maximum/1.763 duration of the pulse and $\mathcal{E}_m$ is the peak of the pulse. We choose $\tau = 50$ fs and $\mathcal{E}_m = 1.73 \times 10^6$ V/m.

C. Incoherent transport

In QCLs, incoherent carrier transport includes electron-LO phonon scattering, electron-electron scattering, electron-interface roughness scattering, electron-acoustic phonon scattering, and electron-impurity scattering. However, for intersubband transitions in QCLs, usually electron-LO phonon scattering dominates other scattering mechanisms by orders of magnitude.[19,20] Electron-electron scattering may become important in cases, where the energy spacing between the levels is smaller than the LO phonon resonance energy, so that electron-LO phonon scattering is forbidden except for the electrons distributed in the high energy tail.[14] Electron-electron scattering also becomes significant in intrasubband transitions.[21] In this work, we calculate the intersubband scattering lifetime $s_{xx'}$ from electron-LO phonon (e-ph) scattering and electron-electron (e-e) scattering, so that

$$1/s_{xx'} = 1/s_{xx'}^{\text{e-ph}} + 1/s_{xx'}^{\text{e-e}}, \tag{4}$$

where $s_{xx'}^{\text{e-ph}}$ and $s_{xx'}^{\text{e-e}}$ are the carrier lifetimes for the transitions from x to x' due to electron-LO phonon scattering and electron-electron scattering, respectively.

D. Coherent transport

Coherent carrier transport between two neighboring quantum wells that are separated by a potential barrier depends on the strength of the coherence ($\Delta_{0,xx'}$), the detuning of the levels from resonance ($E_{xx'}$), and the lifetime of the coherence ($T_{2,xx'}$). Coherent transport and oscillations of the propagating electron wave-packets between the coherently coupled energy levels increase with the increase in $\Delta_{0,xx'}$. To calculate $\Delta_{0,xx'}$, we apply a variable electric field to the QCL and determine the minimum separations between the injector and active region energy levels. Since $\Delta_{0,xx'}$ depends on the height and width of the potential barrier between quantum wells, so does coherent carrier transport. The height of the barrier depends on the choice of materials and the width of the barrier depends on quantum mechanical designs. Coherent carrier transport decreases as $E_{xx'}$ increases. Coherent carrier transport is maximum when $E_{xx'}=0$. Since the phase coherence of the coherently propagating electrons exists for a time $T_{2,xx'}$, coherent transport is efficient when coherence exists for a long time so that $T_{2,xx'} \gtrsim 2\pi\hbar/\Delta_{0,xx'}$.

The propagating electron wave-packets lose phase coherence mainly due to intrasubband electron-LO phonon scattering, electron-electron scattering, and electron-interface roughness scattering.[11,22] The scattering rates depend on the quantum mechanical design, smoothness of the interfaces, carrier density, and temperature, and, therefore, so does the coherence time. The coherence time $T_{2,xx'}$ can be written as

$$\frac{1}{T_{2,xx'}} = \frac{1}{T_{2,xx'}^{\text{e-e}}} + \frac{1}{T_{2,xx'}^{\text{e-ph}}} + \frac{1}{T_{2,xx'}^{\text{e-ir}}}, \tag{5}$$

where $1/T_{2,xx'}^{\text{e-e}}$, $1/T_{2,xx'}^{\text{e-ph}}$, and $1/T_{2,xx'}^{\text{e-ir}}$ are the rates of the decay of the phase coherence due to electron-electron scattering, electron-LO phonon scattering, and electron-interface roughness scattering, respectively. The propagating electrons may lose phase coherence in either of the levels. The scattering of an electron in subband x due to an electron or an LO phonon is uncorrelated with the scattering of an electron in subband x' due to an electron or an LO phonon. Therefore, intrasubband electron-electron and electron-LO phonon transitions in levels x and x' separately contribute to the loss of the phase coherence and the rates add linearly. In our model, we consider the dominant intrasubband electron-electron transitions, i.e., $x,x \rightarrow x,x$ and $x',x' \rightarrow x',x'$, and we neglect the less significant intrasubband electron-electron scattering, such as $x,x' \rightarrow x,x'$, in order to reduce the computational burden. However, we have seen that the results do not change significantly when $x,x' \rightarrow x,x'$ electron-electron scattering is included in the model. Therefore, the rate of the decay of the phase coherence due to electron-electron scattering can be written as

$$\frac{1}{T_{2,xx'}^{\text{e-e}}} = \frac{1}{s_{x,x\rightarrow x,x}^{\text{e-e}}} + \frac{1}{s_{x'x'\rightarrow x'x'}^{\text{e-e}}}, \tag{6}$$

where $s_{x,x\rightarrow x,x}^{\text{e-e}}$ is the scattering lifetime due to $x,x \rightarrow x,x$ electron-electron transitions. While scattering due to LO phonon, an electron may scatter by emitting an LO phonon or by absorbing an LO phonon. Therefore, $T_{2,xx'}^{\text{e-ph}}$ can be written as

$$\frac{1}{T_{2,xx'}^{\text{e-ph}}} = \frac{1}{s_{xx}^{\text{e-ph,abs}}} + \frac{1}{s_{xx}^{\text{e-ph,em}}} + \frac{1}{s_{x'x'}^{\text{e-ph,abs}}} + \frac{1}{s_{x'x'}^{\text{e-ph,em}}}, \tag{7}$$

where $s_{xx}^{\text{e-ph}}$ is the intrasubband scattering lifetime in subband x due to electron-LO phonon transitions, and the superscripts "abs" and "em" denote absorption and emission, respectively. By contrast, the intrasubband transitions due to interface-roughness in levels x and x' are correlated since nonuniformity in an interface causes a change in the energy of all the electrons that have a finite probability of existence near that interface. Therefore, the intrasubband scattering rate in level x and the intrasubband scattering rate in level x' due to interface roughness cannot be linearly added when calculating the coherence time. Instead, we write[22,23]

$$\frac{1}{T_{2,xx'}^{\text{e-ir}}} = \frac{1}{s_{xx}^{\text{e-ir}}} + \frac{1}{s_{x'x'}^{\text{e-ir}}} - 2\frac{1}{\sqrt{s_{xx}^{\text{e-ir}} s_{x'x'}^{\text{e-ir}}}}, \tag{8}$$

where $s_{xx}^{\text{e-ir}}$ is the intrasubband scattering lifetime in subband x due to electron-interface roughness transitions.

The implementation of the gain recovery model starts with the calculations of the quantized energy levels and the associated wave functions of QCLs. To calculate the energy levels and the associated wave functions, we use the effective mass approach in the envelope function approximation and taking nonparabolicity into account.[4] We use the necessary parameter values of the QCL material systems from Ref. 24. The calculated energy levels and the associated wave functions are used to calculate the scattering and coherence lifetimes in Eqs. (1a), (1b), (2a), (2b), and (3). We calculate the electron-LO phonon and electron-electron scattering rates using the approaches that are discussed in Ref. 25, and the electron-interface roughness scattering rate using the approach that is discussed in Ref. 23. The scattering and coherence lifetimes between the energy levels are recalculated as the carrier densities in the energy levels change. To calculate the electron-interface roughness scattering, we assume that the mean height and the correlation length of the roughness are 0.162 nm and 6 nm, respectively. In this work, we assume a temperature of 200 K. We also assume that the electron temperature is equal to the lattice temperature.

III. RESULTS

We have implemented the gain recovery model for the QCLs of Refs. 26 and 27. These two QCLs are quite different in the choice of material systems and quantum mechanical designs. The QCL of Ref. 26 is designed on GaAs/AlGaAs material system. This QCL is designed to have three quantum wells in the active region, diagonal radiative transition, and single-phonon depopulation of the lower lasing

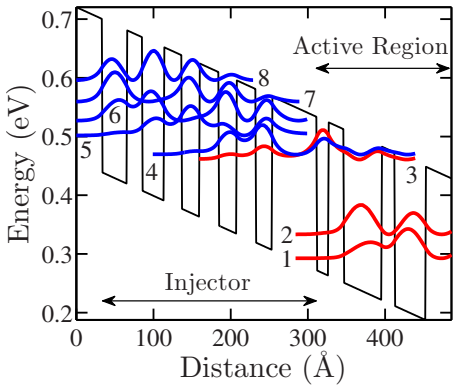

FIG. 1. (Color online) Conduction band diagram and moduli-squared wave functions for the QCL of Ref. 26. The applied electric field is 60 kV/cm.

level. By contrast, the QCL of Ref. 27 is designed on InGaAs/InAlAs material system. This QCL is designed to have four quantum wells in the active region, vertical radiative transition, and double-phonon depopulation of the lower lasing level. These two QCLs represent two types of QCL designs that have been mostly used to date.

A. QCL of Ref. 26

The conduction band diagram and the moduli-squared wave functions for one period of the QCL of Ref. 26 are given in Fig. 1. In Fig. 1, levels 1–3 are in the active region and levels 4–8 are in the injector. The time-resolved solutions of Eqs. (1) and (2) are given in Fig. 2. We note that $n_3 \approx n_4$, $n_2 \approx n_8$, and $n_1 \approx n_7$ at equilibrium, and there are pronounced oscillations in the evolution of n_1, n_2, n_3, n_4, n_7, and n_8 at the start and during the recovery, which indicate the presence of significant coherent tunneling. We also note that $n_3 \gg n_2$ and $n_4 \gg n_5$, n_6, n_7, and n_8. The pump pulse is applied at 6 ps, when the carrier densities are at equilibrium. We note that n_2 increases sharply while n_3 decreases sharply due to the interactions with the pump pulse. As the pump pulse leaves the medium, both n_2 and n_3 recover the equilibrium values. We note that n_2 recovers at a faster rate than n_3. The other energy levels also experience a change in their carrier densities as they are coherently and incoherently coupled to the lasing levels.

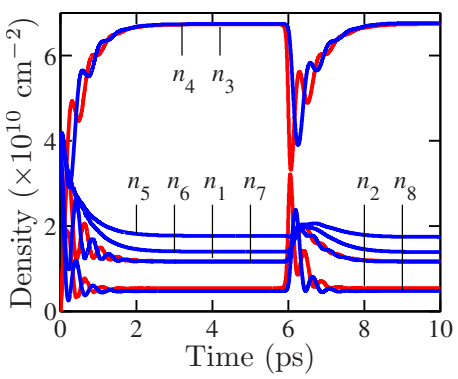

FIG. 2. (Color online) Time evolution of the carrier densities in the energy levels of the QCL of Ref. 26. The temperature is 200 K and the total carrier density per period is 2×10^{11} cm^{-2}.

TABLE I. Key parameter values for gain recovery. (Here, e is charge of an electron.)

QCL of Ref. 26			
s_{43}	1.5 ps		
s_{21}	0.46 ps		
$T_{2,43}$	0.2 ps		
$\Delta_{0,43}$	8.0 meV		
E_{43}	0.5 meV		
η/e	1.6 nm		
$T_{2,32}$	0.12 ps		
QCL of Ref. 27			
s_{64}	5.2 ps	$T_{2,74}$	0.31 ps
s_{74}	5.9 ps	$\Delta_{0,64}$	5.8 meV
s_{84}	2.0 ps	$\Delta_{0,74}$	4.3 meV
s_{54}	1.0 ps	E_{64}	0.6 meV
s_{32}	0.52 ps	E_{74}	7.8 meV
s_{31}	1.33 ps	η/e	2.0 nm
$T_{2,64}$	0.26 ps	$T_{2,43}$	0.06 ps

If the QCL is inverted at equilibrium, the gain recovery will mainly depend on the rates at which carriers are injected into the upper lasing level (level 3) and extracted from the lower lasing level (level 2). The injection and extraction rates depend on the scattering lifetimes and coherent tunneling rates between the injector and active region levels, which will depend on the quantum mechanical design and the operating conditions such as applied electric field and temperature. The key scattering and coherence times, resonant energy splitting, and energy detuning that are responsible for electron injection and extraction for an applied electric field of 60 kV/cm are given in Table I. We note that levels 3 and 4 have a large resonance energy splitting of 8 meV due to the small barrier height of GaAs/AlGaAs material system. We also note that levels 3 and 4 are detuned by only 0.5 meV from resonance when the applied electric field is 60 kV/cm. Therefore, significant coherent carrier transport is expected between levels 3 and 4. At resonance, the carriers will coherently oscillate between levels 3 and 4 with a period $T_{\text{osc}} = 2\pi\hbar/\Delta_{0,34} \approx 0.5$ ps with the coherence decaying at $T_{2,34} = 0.2$ ps. In Fig. 3, we show the pump pulse and the inversion profile $[n_3(t) - n_2(t)]/(n_{3,\text{eq}} + n_{2,\text{eq}})$, where the subscript "eq" denotes equilibrium. The inversion profile directly represents the gain recovery dynamics. In Fig. 3, the gain is

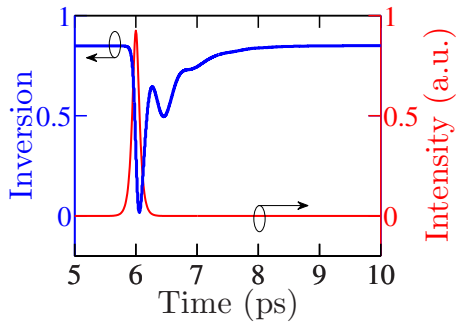

FIG. 3. (Color online) Inversion (gain) recovery of the QCL of Ref. 26 and the pump pulse.

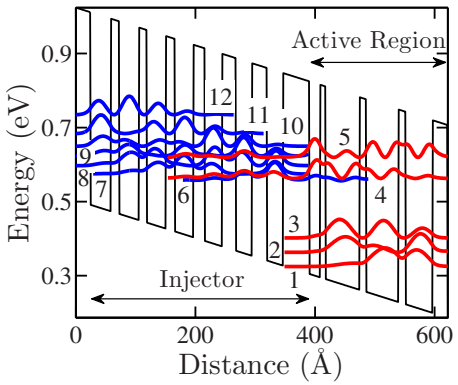

FIG. 4. (Color online) Conduction band diagram and moduli-squared wave functions for the QCL of Ref. 27. The applied electric field is 51 kV/cm.

constant before the pump pulse interacts with the lasing levels. The gain decreases sharply when the pump pulse interacts with the lasing levels. The recovery of the gain begins as the pump pulse leaves the medium. We note two time constants in the gain recovery dynamics, similar to that observed in the pump-probe experiments. Initially, approximately 75% of the gain recovers at a rapid rate in only ~0.25–0.5 ps. This rapid recovery is due to very fast depopulation of level 2, since s_{21} is only 0.46 ps, and coherent tunneling from level 4 to level 3 before the phase coherence between them decays. We note coherent oscillations in the recovery dynamics with a period of approximately 0.5 ps. After this initial rapid recovery, the rate of the gain recovery is slow and the remaining ~25% of the gain recovers in ~1.5–1.75 ps. The coherent oscillations also diminish in the tail of the recovery since $T_{2,34}$ is only 0.2 ps. The gain recovers completely at ~2 ps.

B. QCL of Ref. 27

The conduction band diagram and the moduli-squared wave functions for the QCL of Ref. 27 are given in Fig. 4. In Fig. 4, levels 1–5 are in the active region and levels 6–12 are in the injector. The time-resolved solutions of Eqs. (1) and (2) are given in Fig. 5. We note that the lasing levels are inverted at equilibrium, i.e., $n_4 \gg n_3$. We also note that, in contrast to the previous case, in addition to the injector ground level 6, levels 7 and 8 have a large carrier density in

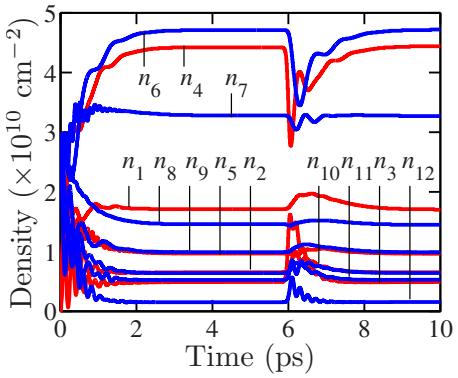

FIG. 5. (Color online) Time evolution of the carrier densities in the energy levels of the QCL of Ref. 27. The temperature is 200 K and the total carrier density per period is 2×10^{11} cm^{-2}.

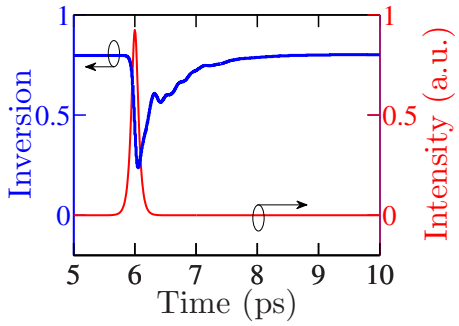

FIG. 6. (Color online) Inversion (gain) recovery of the QCL of Ref. 27 and the pump pulse.

the injector. Level 5, which is a localized level above the upper lasing level (level 4), also has a significant carrier density. Therefore, not only level 6 but also levels 5, 7, and 8 will have significant carrier contributions to level 4. As in the previous case, a pump pulse, which is resonant to the lasing levels 3 and 4, is applied at 6 ps, when the carrier densities are at equilibrium. Due to the interactions with the pump pulse, carrier densities of the lasing levels n_3 and n_4 experience sharp changes. We note coherent oscillations in the recovery of the equilibrium values of the carrier densities.

The pump pulse and the inversion profile $[n_4(t) - n_3(t)]/(n_{4,eq}+n_{3,eq})$ are given in Fig. 6. The key parameter values for the gain recovery at an applied electric field of 51 kV/cm are given in Table I. We note that levels 4 and 6 have a smaller resonance energy splitting of 5.8 meV than that in the previous case due to greater barrier height of InGaAs/InAlAs material system. We also note that levels 4 and 6 are detuned by only 0.6 meV from resonance in an electric field of 51 kV/cm. However, s_{64} is large so that incoherent carrier transport from level 6 to level 4 is relatively slow. On the contrary, s_{54} and s_{84} are small enough for carriers to incoherently scatter from levels 5 and 8 to level 4. On the other hand, levels 7 and 8 have large detuning with level 4 so that the coherent tunneling is negligible. When levels 4 and 6 are at resonance, the carriers coherently oscillate between them with a period $T_{osc} \approx 0.7$ ps with the coherence decaying at $T_{2,46}=0.26$ ps. As in the previous case, we observe two time constants in the gain recovery: A rapid recovery of ~65% of the gain in only ~0.25–0.5 ps is followed by a slow recovery of the remaining ~35% of the gain in ~1.5–1.75 ps. The rapid recovery at the beginning due to mainly very short s_{32} and coherent tunneling from level 6 to level 4. The upper lasing level recovery is relatively slow due to a relatively long s_{64}, s_{74}, s_{84}, and s_{54}, and decay of the coherence. The oscillations in the gain recovery are somewhat irregular in comparison with the previous case since the lasing levels have significant coupling with more than one energy level. However, the gain recovery is ~2 ps in this case too.

IV. CONCLUSION

In conclusion, we have presented a model to calculate the gain recovery of QCLs and implemented the model to calculate the gain recovery of two QCLs that are different in the choice of materials and quantum mechanical designs. We have found that during the recovery, carriers coherently os-

cillate at subpicosecond periodicity with the coherence decaying at ~0.2 ps in both cases. The magnitude of the oscillations, and therefore, the contribution of coherent carrier transport in the gain recovery depends on the strength of coherence. The coherent oscillations in the gain recovery of the QCL of Ref. 26 are more pronounced because of the greater strength of coherence. The incoherent scattering contributions also are different for the two QCLs. In both cases, we observe two distinct time constants in the gain recovery as have been observed in the pump-probe experiments—a relatively fast recovery of most of the gain in the beginning and a relatively slow recovery of the remaining of the gain in the tail, with distinctions in the details of the dynamics.

Both incoherent scattering and coherent tunneling rates depend on the operating conditions, especially, on the temperature. Therefore, the gain recovery dynamics will change when temperature changes.

ACKNOWLEDGMENTS

The author gratefully thanks Professors C. Menyuk, F.-S. Choa, C. Gmachl, A. Johnson, and J. Khurgin for the fruitful discussions.

[1]H. Haus, IEEE J. Sel. Top. Quantum Electron. **6**, 1173 (2000).
[2]F. Capasso, R. Paiella, R. Martini, R. Colombelli, C. Gmachl, T. Myers, M. Taubman, R. Williams, C. Bethea, K. Unterrainer, H. Hwang, D. Sivco, A. Cho, A. Sergent, H. Liu, and E. Whittaker, IEEE J. Quantum Electron. **38**, 511 (2002).
[3]J. Faist, F. Capasso, D. Sivco, C. Sirtori, A. Hutchinson, and A. Cho, Science **264**, 553 (1994).
[4]J. Faist, F. Capasso, C. Sirtori, D. Sivco, and A. Cho, in *Quantum Cascade Lasers in Intersubband Transition in Quantum Wells: Physics and Device Applications II*, edited by H. Liu and F. Capasso (Academic, New York, 2000).
[5]A. Gordon, C. Wang, L. Diehl, F. Kärtner, A. Belyanin, D. Bour, S. Corzine, G. Höfler, H. Liu, H. Schneider, T. Maier, M. Troccoli, J. Faist, and F. Capasso, Phys. Rev. A **77**, 053804 (2008).
[6]M. Talukder and C. Menyuk, Phys. Rev. A **79**, 063841 (2009).
[7]C. Sirtori, F. Capasso, J. Faist, A. Hutchinson, D. Sivco, and A. Cho, IEEE J. Quantum Electron. **34**, 1722 (1998).
[8]F. Eickemeyer, K. Reimann, M. Woerner, and T. Elsaesser, Phys. Rev. Lett. **89**, 047402 (2002).
[9]A. Wacker, Phys. Status Solidi C **5**, 215 (2008).
[10]H. Choi, L. Diehl, Z.-K. Wu, M. Giovannini, J. Faist, F. Capasso, and T. Norris, Phys. Rev. Lett. **100**, 167401 (2008).
[11]M. Woerner, K. Reimann, and T. Elsaesser, J. Phys.: Condens. Matter **16**, R25 (2004).
[12]H. Choi, Ph.D. thesis, The University of Michigan, 2007.
[13]R. Iotti and F. Rossi, Phys. Rev. Lett. **87**, 146603 (2001).
[14]D. Indjin, P. Harrison, R. Kelsall, and Z. Ikonić, J. Appl. Phys. **91**, 9019 (2002).
[15]R. Nelander, A. Wacker, M. Pereira, Jr., D. Revin, M. Soulby, L. Wilson, J. Cockburn, A. Krysa, J. Roberts, and R. Airey, J. Appl. Phys. **102**, 113104 (2007).
[16]T. Kubis, C. Yeh, and P. Vogl, Phys. Status Solidi C **5**, 232 (2008).
[17]R. Terazzi and J. Faist, New J. Phys. **12**, 033045 (2010).
[18]R. Boyd, *Nonlinear Optics*, 2nd ed. (Academic, London, 2003).
[19]R. Ferreira and G. Bastard, Phys. Rev. B **40**, 1074 (1989).
[20]M. Hartig, S. Haacke, B. Deveaud, and L. Rota, Phys. Rev. B **54**, R14269 (1996).
[21]P. Harrison, Appl. Phys. Lett. **75**, 2800 (1999).
[22]A. Wittmann, Y. Bonetti, J. Faist, E. Gini, and M. Giovannini, Appl. Phys. Lett. **93**, 141103 (2008).
[23]T. Unuma, M. Yoshita, T. Noda, H. Sakaki, and H. Akiyama, J. Appl. Phys. **93**, 1586 (2003).
[24]M. Levinshtein, S. Rumyantsev, and M. Shur, *Semiconductor Parameters* (World Scientific, Singapore, 1996).
[25]J. Smet, C. Fonstad, and Q. Hu, J. Appl. Phys. **79**, 9305 (1996).
[26]C. Sirtori, P. Kruck, S. Barbieri, P. Collot, and J. Nagle, Appl. Phys. Lett. **73**, 3486 (1998).
[27]Z. Liu, D. Wasserman, S. Howard, A. Hoffman, C. Gmachl, X. Wang, T. T.-Ek, L. Cheng, and F.-S. Choa, IEEE Photonics Technol. Lett. **18**, 1347 (2006).